THE JOURNAL OF PHYSICAL CHEMISTRY C

Article

pubs.acs.org/JPCC

Rheological Mechanism of Long-Term Self-Assembly in Saponite Nanoparticles

Kiminori Sato,*[,†] Koichiro Fujimoto,[†] Katsuyuki Kawamura,[‡] Weili Dai,[§] and Michael Hunger[∥]

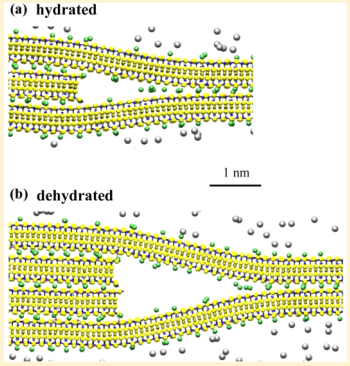
[†]Department of Environmental Sciences, Tokyo Gakugei University, 4-1-1 Koganei, Tokyo 184-8501, Japan

[‡]Graduate School of Environmental Science, Okayama University, Tsushima, Okayama 700-8530, Japan

[§]Key Laboratory of Advanced Energy Materials Chemistry (Ministry of Education), College of Chemistry, Nankai University, Tianjin 300071, P. R. China

[∥]Institute of Chemical Technology, University of Stuttgart, Pfaffenwaldring 55, 70569 Stuttgart, Germany

ABSTRACT: A rheological mechanism of long-term self-assembly induced by H_2O molecules is highlighted for layered saponite nanoparticles based on the results of thermogravimetry and differential thermal analysis, time-resolved length change measurement with high-resolution dilatometry, solid-state nuclear magnetic resonance, positronium annihilation spectroscopy, and molecular dynamics simulation. Prior to self-assembly, saponite nanoparticles exhibit two kinds of local molecular structures, where one and two nanosheets are inserted into interlayer spaces forming open spaces with their sizes of ~0.3 and ~0.9 nm, respectively. H_2O molecules adsorbed at Na^+ cations in the interlayer spaces immediately trigger off the onset of the rheological motion of nanosheets in parallel to the layer direction. One of two nanosheets inserted into the interlayer spaces is thus gradually released away, with the local molecular structure with smaller open spaces getting to dominant for the self-assembled saponite nanoparticles.



1. INTRODUCTION

Nanoparticle self-assembly is a phenomenon, in which nanoscale particles spontaneously agglomerate with well-defined local structures through their mutual interactions.[1] Self-assembly often leads to specific properties and functionalities that cannot be accessible by the conventional technique of material synthesis.[2,3] The application of self-assembly to material synthesis could be thus currently one of the most straightforward strategies that allows the design of new multifunctional nanocomposites,[4] although the phenomenon of self-assembly itself has not yet been understood. In addition, the self-assembly of nanoparticles is increasingly of importance for dealing with the global environmental issues. It has been reported that dynamical functionality in the soil environment emerges as a consequence of self-assembly in the soil-microbe system.[5] In the recent practical model of giant earthquake nucleation, pore fluid of self-assembled geomaterials plays an important role in earthquake slip weakening in plate-boundary faults.[6]

Inorganic layered compounds known as clay minerals are typical materials that exhibit self-assembly in the presence of H_2O molecules.[7,8] They can contain a number of H_2O molecules in the angstrom-scale interlayer spaces, which is characteristic for the swelling property.[9] The high capability of H_2O adsorption is based on the fact that the inorganic layered compound possesses a negative layer charge compensated by interlayer cations attractive to polarized H_2O molecules. Numerous studies on self-assembly of clay nanoparticles have thus been focused on the rheological behavior in aqueous suspension.[10] Layer-by-layer assembly is one of the promising techniques for the fabrication of functional film with respect to the rheology of clay nanoparticles.[11,12] Synchrotron-based small-angle X-ray scattering for clay nanoparticles in aqueous suspension revealed the strong positional and orientational order of nanosheets, which captures the specific gel structure due to attractive interactions among them.[13]

In the present study, the self-assembly of layered-saponite nanoparticles is explored by positronium (Ps) annihilation spectroscopy coupled to thermogravimetry and differential thermal analysis (TG-DTA), time-resolved length change measurement with high-resolution dilatometry, solid-state nuclear magnetic resonance (NMR), and molecular dynamics (MD) simulation. We focus on the long-term self-assembly ranging from the onset of H_2O adsorption at the interlayer cations to far after complete hydration. The purpose of the present work is to answer the following questions: (1) What is the driving force of self-assembly for saponite nanoparticles? (2) Is the self-assembly of saponite nanoparticles rheological? (3) Are there local molecular structures responsible for the self-assembly of saponite nanoparticles?

2. EXPERIMENTAL SECTION

2.1. Materials. Synthetic Na-type saponite nanoparticles (54.71% SO_2, 5.02% Al_2O_3, 0.03% Fe_2O_3, 30.74% MgO, 2.15%

Received: July 25, 2012
Revised: September 21, 2012
Published: October 12, 2012

 © 2012 American Chemical Society dx.doi.org/10.1021/jp307358d | J. Phys. Chem. C 2012, 116, 22954−22959

Na_2O, 0.07% CaO, 0.67% SO_3, 6.64% H_2O) produced by Kunimine Industries, Japan were employed in this study. The particle size is ~45 nm in diameter. The samples were dehydrated at 423 K for 12 h under the vacuum condition of $\sim 10^{-5}$ Torr and are referred to as the starting saponite samples.

2.2. Thermal Analysis. Adsorption of H_2O molecules was investigated with respect to the thermogravity (TG) caused by weight gain. The time-dependent TG data were obtained by TG-DTA system (TG-DTA 2020SA, Bruker AXS) at room temperature with α corundum (α Al_2O_3) as an internal standard. Parallel to that, length-change measurements were performed for the uniaxially compacted samples with a high-precision differential-type dilatometer (TD5020SA, Bruker AXS) equipped with a closed-water-cycling system. The dilatometer system is fully cooled, keeping constant temperature with high thermal stability and preventing overshooting temperature and runaway, which enables us to perform long-term measurements.[14] The starting samples were exposed to the humidity of ~35% at the temperature of ~300 K, where the time-dependent data were obtained.

2.3. Solid-State Nuclear Magnetic Resonance. The solid-state NMR experiments were performed for examining the local structural variation caused by H_2O adsorption using a Bruker Avance III 400WB spectrometer at resonance frequencies of 400.3 MHz for ^1H and 105.8 MHz for ^{23}Na nuclei, respectively. For the ^1H and ^{23}Na magic-angle-spinning (MAS) NMR studies, 4 mm-Bruker rotors were used with sample spinning rates of 10 kHz, $\pi/2$ and $\pi/8$ flip angles, and repetition times of 10 and 0.5 s, respectively. The starting (dehydrated) sample was exposed to the humidity of ~35% at the temperature of ~300 K for 0 min, 15 min, 35 min, 1 h, 2 h, 5 h, and 10 h before recording the ^1H and ^{23}Na MAS NMR spectra.

2.4. Characterization of Open Spaces. The sizes of open spaces and their fractions were investigated by Ps annihilation lifetime spectroscopy.[15−17] A fraction of energetic positrons injected into samples forms the bound state with an electron, positronium (Ps). Singlet *para*-Ps (*p*-Ps) with the spins of the positron and electron antiparallel and triplet *ortho*-Ps (*o*-Ps) with parallel spins are formed at a ratio of 1:3. Hence, three states of positrons−*p*-Ps, *o*-Ps, and free positrons−exist in samples. The annihilation of *p*-Ps results in the emission of two γ-ray photons of 511 keV with lifetime ~125 ps. Free positrons are trapped by negatively charged parts such as polar elements and annihilated into two photons with lifetime ~450 ps. The positron in *o*-Ps undergoes two-photon annihilation with one of the bound electrons with a lifetime of a few nanoseconds after localization in angstrom-scale pores. The last process is known as *o*-Ps pick-off annihilation and provides information on the free volume size R through its lifetime τ_3 based on the Tao−Eldrup model:[18,19]

$$\tau_3 = 0.5\left[1 - \frac{R}{R_0} + \frac{1}{2\pi}\sin\left(\frac{2\pi R}{R_0}\right)\right]^{-1} \quad (1)$$

where $R_0 = R + \Delta R$, and $\Delta R = 0.166$ nm is the thickness of homogeneous electron layer in which the positron in *o*-Ps annihilates. The positron source (^{22}Na), sealed in a thin foil of Kapton, was mounted in a sample−source−sample sandwich. The starting samples were exposed to the humidity of ~35% at the temperature of ~300 K, where the Ps lifetime spectra were obtained every 45 min. The validity of our lifetime measurements and data analysis was confirmed with certified reference materials (NMIJ CRM 5601-a and 5602-a) provided by National Metrology Institute of Japan, National Institute of Advanced Industrial Science and Technology (AIST).[20,21] Positron lifetime spectra were numerically analyzed using the POSITRONFIT code.[22]

2.5. Molecular Dynamics Simulation. The NPT ensemble MD simulations were conducted at 300 K and 0.1 MPa for Ca-saponite with layer charge of $z = 0.333$. Two systems were simulated using MXDORT/MXDTRICL code.[23] Initial structures were prepared as follows:

(1) The sheet structure of Ca-saponite ($z = 0.333e$) was prepared using phlogopite unit cell multiplied by 6 × 36 × 1. The cell lengths of a and b axes were about 3.2 and 33.2 nm, respectively.
(2) The two infinite sheets were stacked.
(3) A sheet of saponite was prepared (6 × 12 × 1) and cut perpendicular to the b axis to make edges. The length of edge to edge was ~11 nm.
(4) One (1-edged system) or two (2-edged system) edged sheets were inserted between the stacked infinite sheets.
(5) 500 argon atoms were placed outside the stacked sheets.

MD calculations were performed with the full EWALD summations for Coulomb interactions and the velocity Verlet algorithm for equations of motion of atoms (time interval = 0.4 fs). Pressure and temperature were controlled by scaling of the periodic cell shape and atom velocities, respectively. The basic cell contained 22 010 (12096O+3696Si+336Al+3018Mg +2028H+336Na+500Ar) atoms for 1-edged system and 25 088 (13824O+4224Si+384Al+3444Mg+2328H+384Na +500Ar) atoms for 2-edged system, respectively.

The following interatomic potential functions were used for all of the atom−atom pairs. A three-body term was added to the H−O−H interaction for intra-atomic and hydrogen bonds because of the sp^3 hybrid orbital.

Two-body central force terms:

$$u_{ij}(r_{ij}) = \frac{z_i z_j e^2}{4\pi\varepsilon_0 r_{ij}} - \frac{c_i c_j}{r_{ij}^6} + f_0(b_i + b_j)\exp\left(\frac{a_i + a_j - r_{ij}}{b_i + b_j}\right) + D_{1ij}\exp(-\beta_{1ij} r_{ij}) + D_{2ij}(-\beta_{2ij} r_{ij}) + D_{3ij}\exp(-\beta_{3ij}(r_{ij} - r_{3ij})^3) \quad (2)$$

Three-body term (angular covalent):

$$u_{jij}(\theta_{jij}, r_{ij}) = -f_k \cos[2(\theta_{jij} - \theta_0) - 1]\sqrt{k_1 k_2} \quad (3)$$

where r is the bond distance, z is the electric charge, and f_0 is the unit conversion constant 6.9511×10^{11} N. The parameters z, a, b, and c for each atom, D_1, D_2, D_3, b_1, b_2, b_3, and r^* (* = 1, 2, and 3) for each atom pair, and f_k, h_0, g_r, and r_m for a three-body term were determined to reproduce the structural and physical properties of several oxide crystals (for example, ice-Ih, ice-II, ice-IX, quartz, corundum, gibbsite, eldspars, muscovite, etc.) and of water. The parameters used in the present study are shown in Table 1. Numerical procedure is described in detail elsewhere.[23]

3. RESULTS AND DISCUSSION

Figure 1a shows the ^1H MAS NMR spectra for saponite nanoparticles recorded after different exposure times ranging from 0 to 10 h. The ^1H MAS spectrum of starting (dehydrated) saponite exhibits a signal of hydroxyl (OH) groups at the

dx.doi.org/10.1021/jp307358d | J. Phys. Chem. C 2012, 116, 22954−22959

Table 1. Parameters for the Inter-Atomic Potential Model

atom	w (10^{-3} kg/mol)	z (e)	a (nm)	b (nm)	c (kJ/mol)$^{-2}$ nm^{-3}
O	16.00	−1.2553	0.1903	0.0150	0.06056
Si	28.90	2.400	0.0908	0.0090	0.0
Al	26.98	2.250	0.1015	0.0080	0.0
H	1.01	0.340	0.0081	0.0044	0.0
Mg	23.305	1.52	1.137	0.01137	0.00442
Ar	39.984	0.0	0.190	0.0133	0.09093
atom−atom	D_1 (kJ/mol)	β_1 (nm)	D_2 (kJ/mol)	β_2 (nm)	
Si−O	34300.0	40.0	−3121.0	20.0	
Al−O	26778.0	40.0	−1936.0	20.0	
H−O	6931.9	55.2	−1442.1	27.6	
atom−atom−atom	f_k (10^{-19} J)	θ_0 (°)	r_m (nm)	g_r (nm^{-1})	
Si−O−Si	6.1	120.0	0.177	168.0	

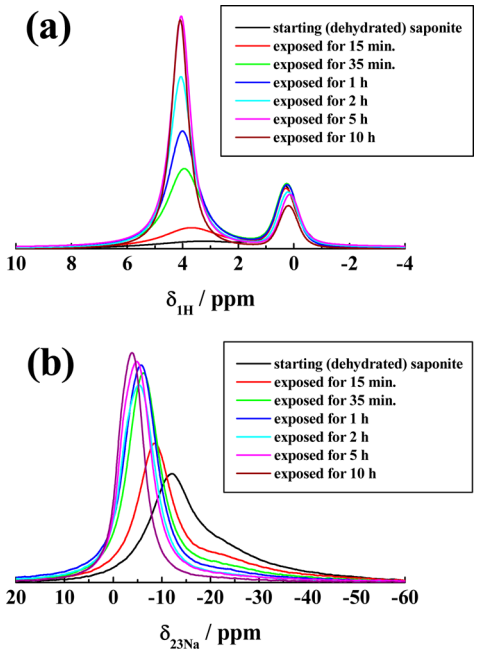


Figure 1. (a) ^{1}H and (b) ^{23}Na MAS NMR spectra of saponite nanoparticles recorded after different exposure times ranging from 0 to 10 h.

chemical shift of 0.3 ± 0.1 ppm. A signal of H_2O begins to appear at the lower chemical shift of 3.4 ± 0.1 ppm at the exposure time of 15 min. The lower chemical shift in comparison with that observed for bulk water in hydrated materials such as in fully hydrated zeolites (4.8 ppm)[24] is caused by water adsorption at surface atoms of the saponite nanoparticles. The structure of H_2O molecules is thus expected to be close to surface water for initially hydrated saponite nanoparticles. The H_2O signal is gradually enlarged together with the peak shift toward to the higher chemical shift up to ~4 ppm with increasing exposure time. This demonstrates that the surface water is altered to the bulk water with increasing hydration degree.

Figure 1b shows the ^{23}Na MAS NMR spectra, in which the effect of H_2O adsorption at Na^+ cations in the interlayer spaces is clearly visible. The ^{23}Na MAS NMR spectrum of the starting (dehydrated) saponite consists of a broad signal centered at −12 ppm with an asymmetric shape, which is determined by the quadrupolar interactions of the resonating ^{23}Na nuclei. This ^{23}Na signal shows a gradual narrowing together with a peak shift toward higher chemical shifts up to −4 ppm with increasing exposure time corresponding to an increasing hydration degree of the saponite nanoparticles. Both of the effects are due to the decreasing electric field gradient in the local structure of the Na^+ cations with increasing water adsorption at these surface sites. The electric field gradient is proportional to the quadrupolar coupling constant of the resonating ^{23}Na nuclei, which is proportional to the broadening and the second-order quadrupolar shift of the ^{23}Na MAS NMR signals.[25] Similar results of ^{1}H and ^{23}Na MAS NMR spectroscopy have been reported for the hydration behavior of zeolite.[24,26]

Figure 2 shows (a) the concentration of H_2O molecules evaluated by comparison of the ^{1}H MAS NMR intensities of

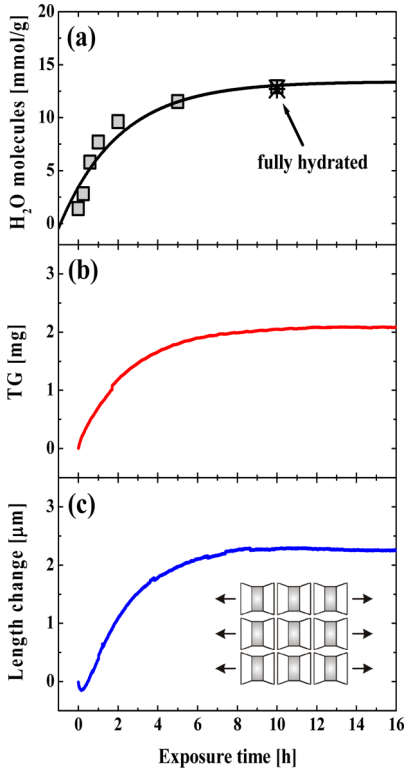


Figure 2. (a) Concentration of H_2O molecules adsorbed at saponite nanoparticles evaluated by comparison of the ^{1}H MAS NMR intensities of the water signals with that of a standard zeolite (solid squares), (b) thermogravity (TG), and (c) length change as a function of exposure time. The black solid line in panel a is drawn for guiding the eye. The star plotted at the exposure time of 10 h in panel a is the data of fully hydrated saponite.

the water signals in Figure 1a with that of a standard zeolite, (b) TG, and (c) length change as a function of exposure time. The concentration of H_2O molecules increases with increasing exposure time up to ~8 h and stays constant above that. The data at 10 h in Figure 2a are essentially the same as that of fully hydrated sample, indicating that adsorption of H_2O molecules at Na^+ cations in the interlayer spaces due to hydration is completed. Similarly to the solid-state NMR data, the TG increases with exposure time up to ~8 h owing to hydration in the interlayer spaces and is saturated thereafter. (See Figure 2b.) The concentration of H_2O molecules estimated from the weight gain of ~2 mg with the molecular weight of 18 g/mol is

dx.doi.org/10.1021/jp307358d | J. Phys. Chem. C 2012, 116, 22954−22959

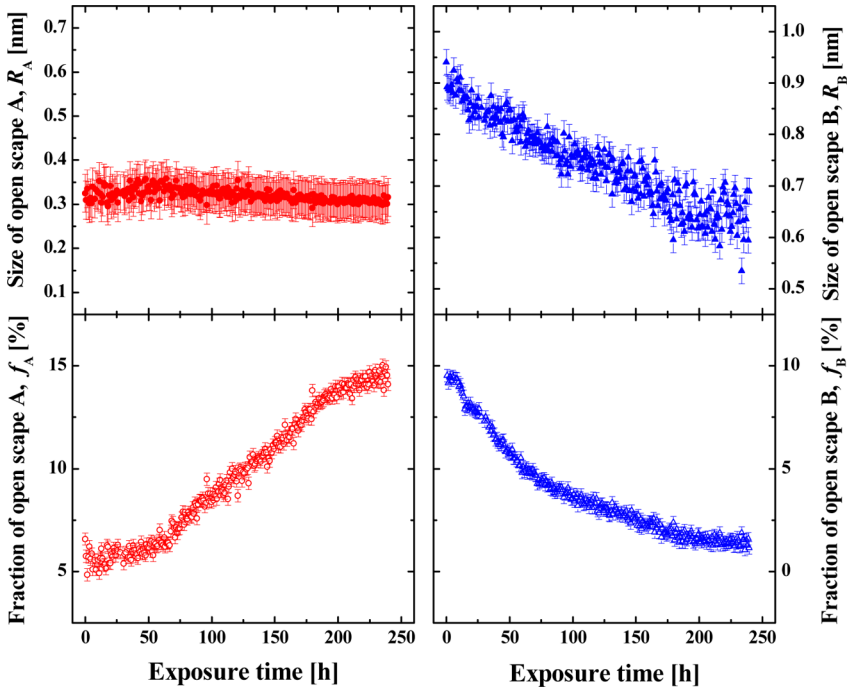


Figure 3. Sizes of open spaces R_A (solid circles in upper left) and R_B (solid triangles in upper right) with their fractions f_A (open circles in lower left) and f_B (open triangles in lower right) as a function of exposure time.

~11 mmol/g, which is in agreement with that deduced from the solid-state NMR data. This is evidence that the weight gain observed by TG-DTA is solely contributed from H_2O adsorption at Na^+ cations in the interlayer spaces. Interestingly, the macroscopic length change due to volume expansion exhibits a time scale similar to those of the NMR and TG-DTA data microscopically occurring at interlayer spaces. (See Figure 2c.) As mentioned above, the present saponite samples are uniaxially compacted for the length-change measurements. It is thus expected that the layer nanosheets are well-ordered, as illustrated as an inset in Figure 3c. H_2O adsorption in the interlayer spaces locally expands basal spacing, as has been assessed by X-ray diffraction (XRD) under the controlled condition of relative humidity.[27] Expansion of basal spacing in the well-ordered layer nanosheets significantly influences the macroscopic length change. It is therefore reasonable that the data of time-dependent length change is synchronized with those of solid-state NMR and TG-DTA.

Ps annihilation spectroscopy reveals two kinds of open spaces denoted as A and B. In Figure 3, the sizes of open spaces R_A and R_B with their fractions f_A and f_B are presented as a function of exposure time, respectively. For the starting (dehydrated) saponite, the open space sizes R_A and R_B are ~0.3 and ~0.9 nm with their corresponding fractions of $f_A \approx 5\%$ and $f_B \approx 10\%$, respectively. The open space size R_A is consistently ~0.3 nm without any significant change along with exposure time, whereas R_B decreases from ~0.9 to ~0.6 nm. The fraction f_A gradually increases from ~5 to ~15% with exposure time in contrast with the decrease in f_B from ~10 to ~2%. The time-dependent data of R_B, f_A, and f_B are well-synchronized on the time scale with ~10 days much longer than those of solid-state NMR, TG-DTA, and volume expansion with ~8 h. We conclude that the long-term MD probed by Ps annihilation spectroscopy originates from the self-assembly of saponite nanoparticles rheologically caused by H_2O molecules.

Our next concern is where the two kinds of open spaces are located in the present saponite nanoparticles under study. The interlayer spaces for the dehydrated saponite completely shrink Na^+ cations, filling up the hexagonal cavity of silicate tetrahedron, as confirmed by XRD experiments.[27] In general, they expand together with H_2O molecules adsorbed at the Na^+ cations in the interlayer spaces as a result of hydration. It is thus unlikely that the open space A with the constant size of ~0.3 nm corresponds to the interlayer spaces. The open space B with its size ranging from ~0.6 to ~0.9 nm is in turn too large to relate to the interlayer spaces. Figure 4 shows the results of MD simulations, addressing the locations of two kinds of open spaces observed by Ps annihilation spectroscopy. MD calculations simulate two kinds of local molecular structures for 1-edged and 2-edged systems respectively, where one- and two-clay nanosheets are inserted into the interlayer spaces, forming nanometer-scale open spaces. It should be noted here that the sizes of open spaces simulated by MD calculations are in excellent agreement with those observed by Ps annihilation spectroscopy. We call the molecular structures of one- and two-nanosheet insertion types with smaller and larger open spaces simply as type A and B, respectively.

Of great surprise is that Ps annihilation spectroscopy in combination with MD simulations specifically reveals the local structures generally unconsidered for the molecular model of inorganic layered materials. Such molecular structures with the nanosheet cross section could not be observed for structurally disordered saponite nanoparticles consisting of light elements, even by high-resolution transmission electron microscopy (TEM). The local molecular structure denoted as the type A with the smaller open space increases, maintaining its size along with self-assembly. The local structure of the type B disappears with self-assembly shrinking its larger open space. The size of open space in the type B approaches that of smaller open space in the type A. The type A is thus an intrinsic local molecular structure of saponite nanoparticles, whereas the type B is a

dx.doi.org/10.1021/jp307358d | J. Phys. Chem. C 2012, 116, 22954−22959

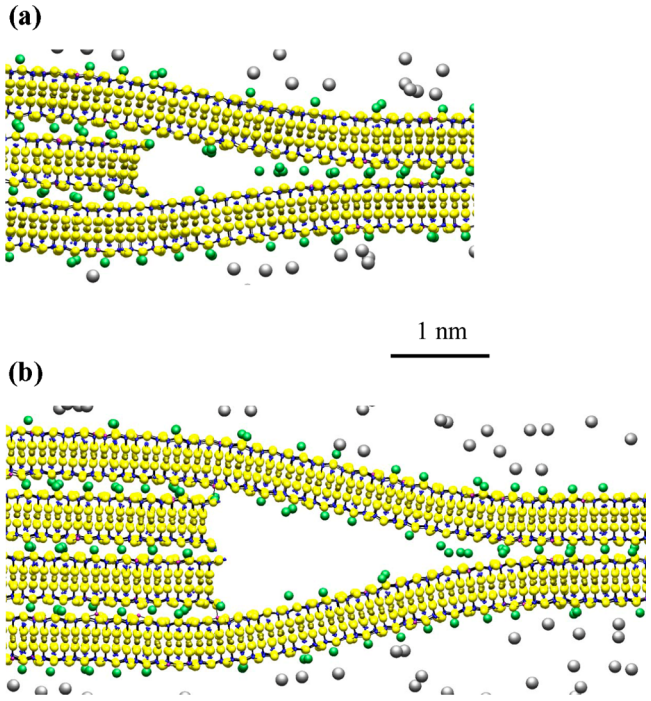


Figure 4. Molecular dynamics (MD) simulated local molecular structures formed by (a) one- and (b) two-nanosheet insertion into the interlayer spaces as 1- and 2-edged systems, respectively.

metastable structure present dominantly prior to self-assembly. It is reasonably inferred that the metastable structure of type B is gradually altered to the intrinsic structure of type A together with self-assembly.

On the basis of the present findings of TG-DTA, ^{1}H and ^{23}Na MAS NMR, Ps annihilation spectroscopy, and MD simulation, the following rheological mechanism of self-assembly induced by H_2O molecules can be drawn for saponite nanoparticles. Prior to self-assembly, saponite nanoparticles possess two kinds of local molecular structures, where one and two nanosheets are inserted into the interlayer spaces, forming the open spaces with their sizes of ∼0.3 and ∼0.9 nm, respectively. The local structures with smaller and larger open spaces correspond to the intrinsic and metastable molecular environments, respectively. Owing to hydration, H_2O molecules begin to adsorb at Na^+ cations in the interlayer spaces with their structures close to surface water. The surface water is altered to the bulk water to complete hydration within ∼8 h. Even at the lower concentration of ∼3 mmol/g, H_2O molecules significantly trigger off the self-assembly of saponite nanoparticles. H_2O molecules adsorbed at the Na^+ cations in the interlayer spaces act as a lubricant, causing the driving force for the rheological motion of nanosheets in parallel to the layer direction. One of two nanosheets inserted into the interlayer spaces is thus released away. The local molecular structures with the larger open spaces are gradually altered to those with the smaller open spaces that finally get to dominant for the self-assembled saponite nanoparticles.

4. CONCLUSIONS

The rheological mechanism of long-term self-assembly induced by H_2O molecules was investigated for layered-saponite nanoparticles. ^{1}H and ^{23}Na MAS NMR spectroscopy together with TG-DTA revealed that H_2O molecules are solely adsorbed at Na^+ cations in interlayer spaces. The hydration in the interlayer spaces completed at the H_2O concentration of 11 mmol/g within 8 h, significantly influencing the macroscopic volume expansion. Prior to self-assembly, saponite nanoparticles possess two kinds of local molecular structures, where one and two nanosheets are inserted into the interlayer spaces forming the open spaces with their sizes of ∼0.3 and ∼0.9 nm, respectively. H_2O molecules in the interlayer spaces due to hydration immediately trigger off the onset of rheological motion of nanosheets in parallel to the layer direction. One of two nanosheets inserted into the interlayer spaces is thus gradually released away, with the local molecular structure with smaller open spaces getting to dominant for the self-assembled saponite nanoparticles. It is beneficial to detect the molecular environment containing the edge site of clay nanosheet specifically by Ps annihilation spectroscopy combined with MD simulation in the present study. This site has not been identified by other techniques as, for example, TEM and XRD, thus having been unconsidered for the molecular model of inorganic layered nanoparticles so far. It is expected that the edge site is chemically active as that of cup-stacked carbon nanotube. The present findings are therefore of particular importance for further experimental approaches with respect to multifunctional catalytic and adsorption materials in addition to the proper treatment of global environmental issues.

AUTHOR INFORMATION

Corresponding Author

*E-mail: sato-k@u-gakugei.ac.jp.

Notes

The authors declare no competing financial interest.

ACKNOWLEDGMENTS

Fruitful discussion with Y. Kobayashi (National Institute of Advanced Industrial Science and Technology) is greatly appreciated. K.S. thanks Alexander von Humboldt Foundation (AvH), Fachbereich Physik der Universitaet Stuttgart, and Max-Planck-Institute fuer Festkoerperforschung for their financial support. This work was partially supported by a Grant-in-Aid of the Japanese Ministry of Education, Science, Sports and Culture (grant nos. 23740234 and 24540485).

REFERENCES

(1) Whitesides, G. M.; Grzybowski, B. *Science* **2002**, *295*, 2418−2421.
(2) Wu, L.; Lal, J.; Simson, K. A.; Burton, E. A.; Luk, Y. Y. *J. Am. Chem. Soc.* **2009**, *131*, 7430−7443.
(3) Toma, L. M.; Gengler, R. Y. N.; Cangussu, D.; Pardo, E.; Lloret, F.; Rudolf, P. *J. Phys. Chem. Lett.* **2011**, 2004−2008.
(4) Garnweitner, G.; Smarsly, B.; Assink, R.; Ruland, W.; Bond, E.; Brinker, C. J. *J. Am. Chem. Soc.* **2003**, *125*, 5626−5627.
(5) Young, I. M.; Crawford, J. W. *Science* **2004**, *304*, 1634−1637.
(6) Wibberley, C. A. J.; Shimamoto, T. *Nature* **2005**, *436*, 689−692.
(7) Balnois, E.; Durand-Vidal, S.; Levitz, P. *Langmuir* **2003**, *19*, 6633−6637.
(8) Lotsch, B. V.; Ozin, G. A. *ACS Nano* **2008**, *2*, 2065−2074.
(9) Porion, P.; Michot, L. J.; Faugére, A. M.; Delville, A. *J. Phys. Chem. C* **2007**, *111*, 5441−5453.
(10) Bandyopadhyay, R.; Liang, D.; Yardimci, H.; Sessoms, D. A.; Borthwick, M. A.; Mochrie, S. G. J.; Harden, J. L.; Leheny, R. L. *Phys. Rev. Lett.* **2004**, *93*, 2283021−2283024.
(11) Decher, G. *Science* **1997**, *277*, 1232.
(12) Glinel, K.; Laschewsky, A.; Jonas, A. M. *J. Phys. Chem. B* **2002**, *106*, 11246−11252.

(13) Michot, L. J.; Bihannic, I.; Maddi, S.; Funari, S.; Baravian, C.; Levitz, P.; Davidson, P. *Proc. Natl. Acad. Sci. U.S.A.* **2006**, *103*, 16101−16104.
(14) Sato, K.; Sprengel, W. *J. Chem. Phys.* **2012**, *137*, 104906-1−104906-7.
(15) Sato, K.; Murakami, H.; Ito, K.; Hirata, K.; Kobayashi, Y. *Macromolecules* **2009**, *42*, 4853−4857.
(16) Sato, K.; Fujimoto, K.; Nakata, M.; Hatta, T. *J. Phys. Chem. C* **2011**, *115*, 18131−18135.
(17) Sato, K. *J. Phys. Chem. B* **2011**, *115*, 14874−14877.
(18) Tao, S. J. *J. Chem. Phys.* **1972**, *56*, 5499−5510.
(19) Eldrup, M.; Lightbody, D.; Sherwood, J. N. *Chem. Phys.* **1981**, *63*, 51−58.
(20) Ito, K.; Oka, T.; Kobayashi, Y.; Shirai, Y.; Saito, H.; Honda, Y.; Nagai, Y.; Fujinami, M.; Uedono, A.; Sato, K.; et al. *J. Appl. Phys.* **2008**, *104*, 0261021−0261023.
(21) Ito, K.; Oka, T.; Kobayashi, Y.; Shirai, Y.; Wada, K.; Matsumoto, M.; Fujinami, M.; Hirade, T.; Honda, Y.; Hosomi, H.; et al. *Mater. Sci. Forum* **2009**, *607*, 248−250.
(22) Kirkegaard, P.; Eldrup, M. *Comput. Phys. Commun.* **1974**, *7*, 401−409.
(23) Nakano, M.; Kawamura, K.; Ichikawa, Y. *Appl. Clay Sci.* **2003**, *23*, 15−23.
(24) Hunger, M.; Freude, D.; Pfeifer, H. *J. Chem. Soc., Faraday Trans. 1* **1991**, *87*, 657−662.
(25) Freude, D. Quadrupolar Nuclei in Solid-State Nuclear Magnetic Resonance. In *Encyclopedia of Analytical Chemistry*; Meyers, R. A., Ed; J. Wiley & Sons: Chichester, U.K., 2000; pp 12188−12225.
(26) Klein, H.; Fuess, H.; Hunger, M. *J. Chem. Soc., Faraday Trans.* **1995**, *91*, 1813−1824.
(27) Morodome, S.; Kawamura, K. *Clays Clay Miner.* **2009**, *57*, 150−160.